1   **Title:** High riverine CO_2 emissions at the permafrost boundary of Western Siberia

2

3   **Authors:** S. Serikova[1]*, O.S. Pokrovsky[2], P. Ala-Aho[3], V. Kazantsev[4], S.N. Kirpotin[5],

4   S.G. Kopysov[5], I.V. Krickov[5], H. Laudon[6], R.M. Manasypov[5,7], L.S. Shirokova[2,7], C. Soulsby[3],

5   D. Tetzlaff[3] and J. Karlsson[1]

6

7   [1]Climate Impacts Research Centre (CIRC), Department of Ecology and Environmental Science,

8   Umeå University, Linnaeus väg 6, 901 87 Umeå, Sweden.

9   [2]GET UMR 5563 CNRS, Geoscience and Environment, University of Toulouse, 14 Avenue

10   Edouard Belin, 314 00 Toulouse, France.

11   [3]University of Aberdeen, Kings College, Old Aberdeen, AB24 3UE Aberdeen, Scotland.

12   [4]Organization of the Russian Academy of Sciences A.M. Obukhov Institute of Atmospheric

13   Physics RAS, Pyzhyovskiy pereulok 3, 119 017 Moscow, Russia.

14   [5]Institute of Monitoring of Climatic and Ecological Systems (IMCES) SB RAS, Akademichesky

15   Avenue 10/3, 634 055, Tomsk, Russia.

16   [6]Department of Forest Ecology and Management, The Swedish University of Agricultural

17   Sciences, Skogsmarksgränd, 901 83 Umeå, Sweden.

18   [7]N. Laverov Federal Center for Integrated Arctic Research, IEPS, Russian Academy of Sciences,

19   23 Nab. Sev. Dviny, Arkhangelsk, Russia.

20

21 **Abstract:** The fate of the vast stocks of organic carbon stored in permafrost of the Western

22 Siberian Lowland (WSL), the world's largest peatland, is uncertain with the magnitude of

23 greenhouse gas emissions from rivers constituting a major unknown. Here we show the first

24 estimates of annual CO_2 emissions from rivers (n=58) across all permafrost zones of WSL (56-

25 67°N), peaking at the permafrost boundary and decreasing with increasing permafrost extent and

26 colder climate conditions. The CO_2 emissions were high and on average 2-times greater than

27 downstream carbon export. High emission and emission to export ratios are attributed to warm

28 temperatures and long transit times of river water. The study shows the important role of WSL

29 rivers in degassing terrestrial carbon prior to its transport to the Arctic Ocean and suggests that

30 changes in both temperature and precipitation are important for understanding and predicting

31 high-latitude river CO_2 emissions in a changing climate.

32

33 **Text:** Large quantities of organic carbon (OC) are stored in permafrost soils in high-latitude

34 regions[1–3]. Recent climate scenarios predict amplified warming of these regions resulting in

35 substantial increase in mean annual air temperatures (MAAT). Such increase will induce

36 widespread permafrost thaw, accelerate release of OC[4] and stimulate its breakdown to carbon

37 dioxide (CO_2) and methane (CH_4) in soils and wetlands[5–7]. Permafrost thawing also increases

38 active layer depth and associated release of OC to adjacent running waters[6], where it is partly

39 mineralized and evaded, mainly as CO_2, to the atmosphere. Outgassing of CO_2 from running

40 waters is of significance in the global C cycle[6,8,9]. Yet, the magnitude of river CO_2 emissions is

41 often overlooked, especially in permafrost-affected landscapes where the consequences of

42 climate warming are predicted to be the most severe[3]. Ignoring high-latitude river CO_2 emissions

43 may therefore cause errors in regional and global C budgets and bias assessments of concurrent

44 changes following permafrost thaw.

45 While measurements of C export by major Arctic rivers are relatively common[10,11] the direct

46 measurements of CO_2 emissions from high-latitude rivers are scarce. Available data show that

47 high-latitude rivers are supersaturated in CO_2 and are hotspots for CO_2 release to the

48 atmosphere[12–14]. Bioassays and small scale field studies suggest that OC released from thawing

49 permafrost can be largely degraded in recipient aquatic systems[15,16]. Furthermore, rivers receive

50 and degas CO_2 derived from soil respiration[17], a process accelerated by permafrost thaw[7,18].

51 Consequently, river CO_2 emissions are important not only for understanding the land-water C

52 exchange with the atmosphere, but also in discerning the degree to which terrestrial C is lost in

53 the aquatic network or exported to downstream coastal areas. This lack of knowledge is

54 particularly evident for Siberia with its extensive permafrost coverage and associated vast C

55 stocks[1]. In fact, WSL alone contains 70 Pg C in the region's extensive peatlands[19,20] and is home

56 to the Arctic's largest watershed, the Ob' River, which is the 2nd largest freshwater contributor to

57 the Arctic Ocean[21]. Moreover, permafrost in WSL is most vulnerable to thaw since its

58 temperature has increased regionally by more than 1°C during the last 30 years[22]. It has been

59 shown recently that WSL permafrost is actively degrading not only within its forest-tundra

60 subzone, but also in its northern tundra subzone[22]. Given the overall sensitivity of permafrost

61 areas to warming, there is a clear need for empirical estimates of CO_2 emissions from

62 permafrost-draining rivers, not least in WSL, to assess their role in regional and global C cycles

63 and the climate system.

64 To quantify and compare rates of CO_2 emissions from rivers across different permafrost zones,

65 we examined 58 rivers spanning a latitudinal gradient from 56 to 67°N and covering an area of

66   ca 1 million km^2 in WSL (Fig. 1). The rivers had no systematic variation in size or discharge

67   along the latitudinal gradient (Extended Data Fig. 1). We carried out *in-situ* measurements of

68   pCO_2 concentrations and deployed floating chambers[23] to estimate instantaneous CO_2 emissions

69   during spring and summer 2015. All rivers, across all permafrost zones, were supersaturated in

70   pCO_2 with similar concentrations both in spring (2402 to 5072 µatm) and summer (2187 to 5328

71   µatm) (Extended Data Table 1, Supplementary Materials Table 2). The CO_2 emissions varied

72   among the zones (1.9 to 12 g C m^{-2} d^{-1} in spring, 2.7 to 7.6 g C m^{-2} d^{-1} in summer) and showed

73   seasonal differences in the permafrost-free and sporadic permafrost zones (Extended Data Fig. 2,

74   Extended Data Table 1, Supplementary Materials Table 3). We also estimated diffusive CH_4

75   emissions from the studied rivers (Extended Data Table 1). Although all rivers were net sources

76   of CH_4 to the atmosphere, these emissions were low with a minor contribution to total

77   atmospheric C emissions, which were dominated by CO_2 (98%).

78   We found strong patterns in annual CO_2 emissions among rivers located in different permafrost

79   zones ($F_{3,54} = 6.808$, $P < 0.05$), with 3 to 5-times greater emissions from rivers where permafrost

80   extent was less than 50%, i.e. the permafrost-free and sporadic, compared to the continuous

81   permafrost zone (Fig. 2). The annual river CO_2 emissions increased with mean annual air

82   temperature (MAAT) throughout permafrost zones (n = 47, $r^2 = 0.27$, $F_{1,47} = 17.3$, $P < 0.05$).

83   Importantly, the peak of annual river CO_2 emissions was observed in the sporadic permafrost

84   zone, with the mean value of 1.65 kg C m^{-2} yr^{-1}, which gradually decreased to 0.36 kg C m^{-2} yr^{-1}

85   in the continuous permafrost zone (Fig. 2). Interestingly, this peak occurs at -2 to -4°C MAAT,

86   which coincides with -2°C MAAT isotherm reported by other studies[24–26] marking the border of

87   permafrost appearance. Together the data suggest that warming will result in a general increase

88   in CO_2 emissions from WSL rivers. There are only limited data available on CO_2 emissions from

89 permafrost-draining rivers, but the mean CO_2 emissions for the WSL rivers are 1.5 to 2 times

90 greater than CO_2 emissions reported for rivers in Alaska[12] and Eastern Siberia[13]. A likely

91 explanation for such difference is the overall greater OC content of WSL soils[2,24–27] compared to

92 Alaska and Eastern Siberia, where soils are more minerogenic[12,13].

93 Our data suggest that a range of climate-dependent factors interact and control CO_2 emissions

94 across WSL. Increasing MAAT (Fig. 3) likely elevates CO_2 emissions because of strong

95 temperature dependency of mineralization rates of OC in rivers, but also by extending the ice-

96 free period (Fig. 3) and thus the time window for atmospheric gas exchange. Higher

97 temperatures can also result in elevated CO_2 emissions via deeper active layers and enhanced

98 export of terrestrial C[11,25,28]. In fact, there is a trend in terrestrial C export (DOC + DIC) with the

99 greatest values observed in the sporadic permafrost zone, where we also see a peak in annual

100 CO_2 emissions from rivers. Yet the differences among the zones are not significant (Extended

101 Data Table 2, $H = 4.5755$, $P > 0.05$), suggesting that climate impacts on CO_2 emissions are

102 mediated mainly via temperature control of internal OC processing rather than the magnitude of

103 terrestrial C supply. Other factors including nutrients and organic matter quality could not

104 explain observed differences in CO_2 emissions across permafrost zones (Supplementary Table

105 3). However, changes in terrestrial C export likely play a role in explaining nonlinear patterns in

106 CO_2 emissions, where the general increase in CO_2 emissions with MAAT throughout permafrost

107 zones reaches a threshold followed by a decrease in the permafrost-free zone despite higher

108 MAAT and longer ice-free period. Although our study was not designed to examine controls on

109 terrestrial C export across permafrost gradient of WSL, indicators of water flow pathways based

110 on stable water isotopes (δ^2H and $\delta^{18}O$) (Extended Data Fig. 3) suggest deeper and longer

111 hydrological flow paths[29] in permafrost-free area, which previously have been shown to lower

112   terrestrial C export as a result of OC retention and adsorption in mineral soils[25,30,31]. Thus, lower

113   terrestrial C export can possibly explain the corresponding reduction in CO_2 emissions from

114   permafrost-free rivers. Yet, more in-depth studies are needed to provide a better mechanistic

115   understanding of the control of C cycling and CO_2 emissions from WSL rivers.

116   To assess the quantitative importance of CO_2 emissions from WSL rivers, we compared annual

117   river CO_2 emissions with river C export across different permafrost zones. We observed overall

118   high emission to export ratios (2 ± 2.2, mean ± interquartile range) and especially so in the

119   southern permafrost zones, where annual river CO_2 emissions are up to 1.7 - 3 -times greater

120   than river C export (Fig. 2, Extended Data Table 2). The low availability of data from other

121   permafrost-affected systems limits our ability to draw firm conclusions, but the ratios for WSL

122   rivers are relatively high compared to the Yukon River[12] (1:1) and also exceed mean ratios

123   (1.3:1) for the global inland waters (Fig. 2). Surprisingly, results for some of the WSL rivers

124   resemble ratios found in the Amazon River (6:1)[12,32]. Although the ratios for WSL rivers contain

125   uncertainties and absolute values should be treated with caution, the results are important and

126   highlight the major role of rivers in the C cycle of WSL. The differences also emphasize the

127   overall diversity in C dynamics across high-latitude rivers and its potential response to climate

128   change.

129   High emission to export ratios are unexpected for permafrost-draining rivers, where colder

130   temperatures should constrain mineralization of exported terrestrial OC in recipient waters[12].

131   Here we suggest that high emission to export ratios of WSL rivers are a result of long travel

132   times of river water, governed by the overall flat topography of the area[31,33,34], which allows

133   sufficient time for mineralization and outgassing to occur. This effect may be further facilitated

134   by a relatively high degradability of terrestrial OC exported from deeper active layers[15,16],

135   resulting in high total mineralization losses of exported terrestrial OC in the aquatic networks of

136   WSL. Shorter water travel times, in addition to direct temperature effects on mineralization rates,

137   may also explain the tendency of decreasing emission to export ratios in the northern rivers of

138   WSL (Fig. 2). In terms of hydrology, WSL exhibits relatively uniform precipitation (515 ± 80,

139   mean $\pm$ interquartile range), but lower temperatures in the north decrease evapotranspiration,

140   thus resulting in increasing runoff (Fig. 3) and shorter water travel times. Further, longer ice-

141   cover period in the north implies that the majority of runoff is restricted to a short time window

142   limiting OC mineralization and subsequent CO_2 release. Temperature therefore not only affects

143   C export and processing, but also water travel times by determining the length of the ice-free

144   period and the magnitude of runoff. Again, the permafrost-free zone did not follow the general

145   trend and showed rather low emission to export ratios, despite higher temperatures and longer

146   water travel times. Here low emission to export ratios could be a result of decreased terrestrial

147   OC vs. IC export due to deeper water flow pathways[11]. Although we do not have data on the

148   terrestrial C export ratios, we observed lower DOC:DIC ratios in the permafrost-free zone[31]

149   (Extended Data Table 1), where higher inorganic fraction of terrestrial C export implies weaker

150   direct temperature and hydrological control of emission to export ratios. This study therefore

151   highlights a complex climate regulation of C cycling in high-latitude rivers where not only

152   changes in temperature *per se*, but also changes in hydrological conditions are likely to control

153   river CO_2 emissions and emission to export ratios in a changing climate.

154   Based on our results we propose a conceptual framework for understanding changes in CO_2

155   emissions and downstream C export in permafrost-draining rivers with warming (Fig. 4).

156   Warming will raise water temperatures and extend river water travel times, which together will

157   increase CO_2 emissions and emission to export ratios from river networks. The important role of

158   water travel times suggests that not only changes in temperature, but also in precipitation will

159   enhance differences in river C fluxes and should be accounted for in assessments of climate

160   change impacts. Also, warming and concurrent active layer deepening will likely stimulate

161   terrestrial C export, further increasing river CO_2 emissions. Importantly, as warming progresses

162   and permafrost thaws, deeper flow pathways will possibly decrease terrestrial C export,

163   overriding positive impacts of temperature and water travel times, and therefore resulting in

164   lower CO_2 emissions from rivers. An important implication of this concept is that any warming-

165   induced change in terrestrial C export is largely offset by active processing and degassing in the

166   river network, leaving river C export to the Arctic Ocean relatively unaffected. This stresses the

167   limitation of relying on lateral river C fluxes as an indicator of change in permafrost regions, and

168   instead advocates for concentrated efforts to assess magnitude and climate control on C
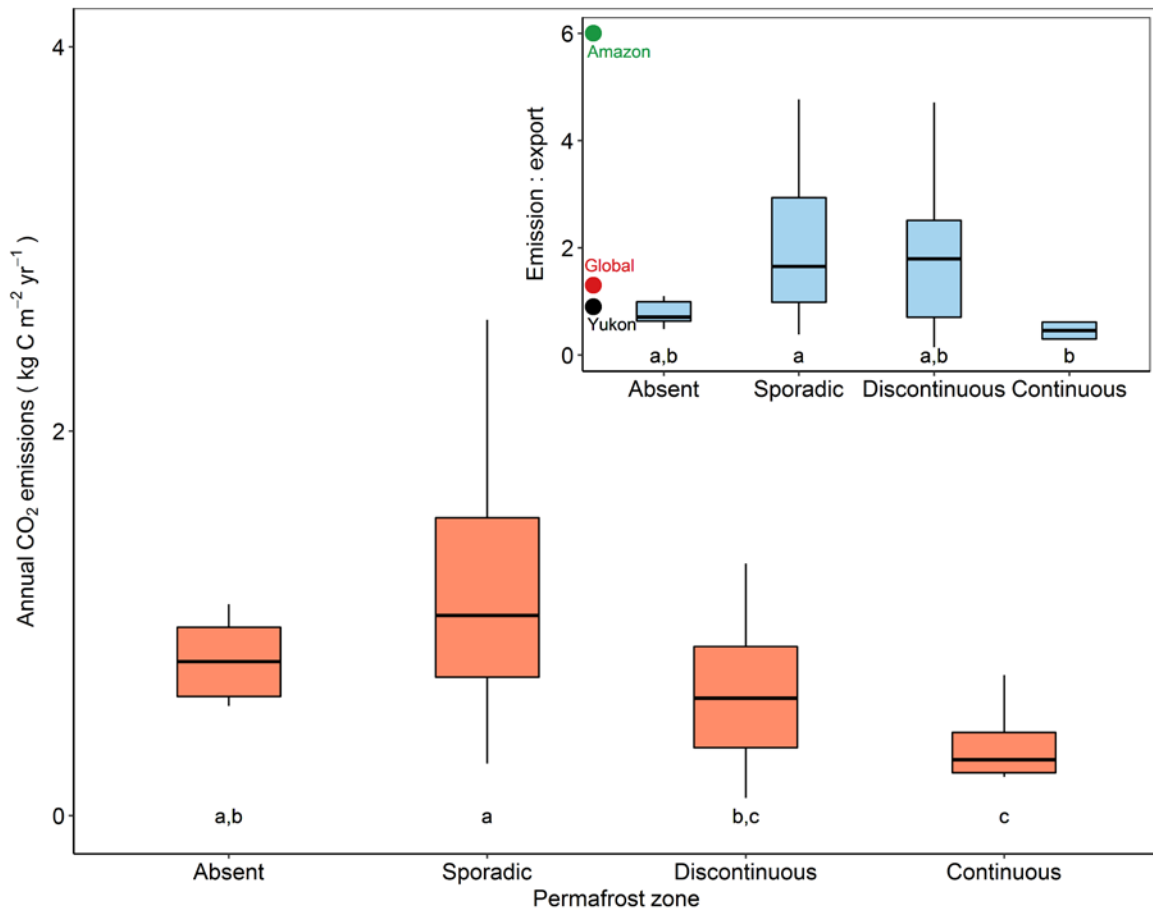
169   emissions from rivers at high latitudes.

170

171
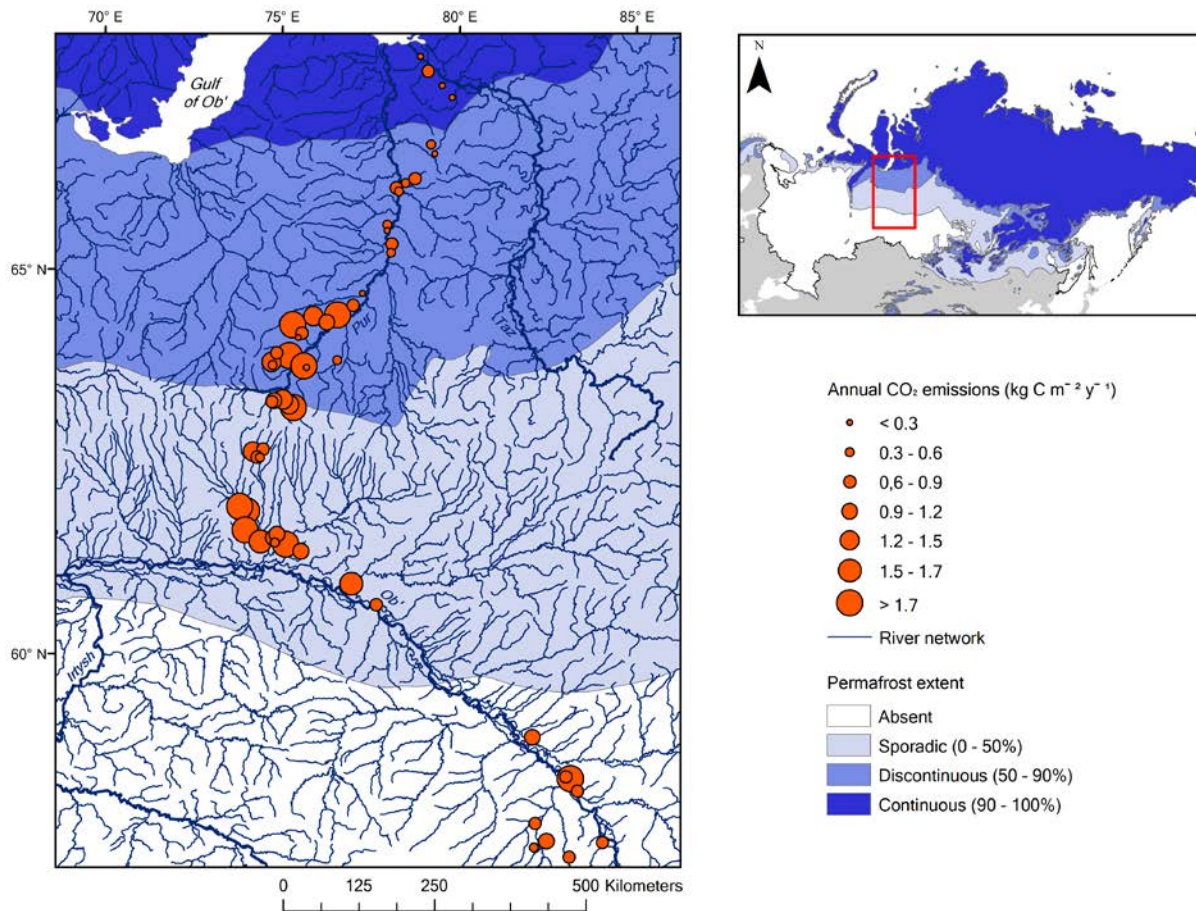
Fig. 1. Map of the study sites in the Western Siberian Lowland, Russia. Based on Brown et al.[35] and Vonk et al.[6]. The size of the orange circles represents the magnitude of the annual CO_2 emissions (per unit water area) from the studied rivers.

175

176

Fig. 2. Annual river CO₂ emissions per unit water area across different permafrost zones.

Boxes are bound by 25th and 75th percentiles and whiskers show 1.5 interquartile range (IQR). Solid line represents median values while crosses indicate outliers. Permafrost zones that share a letter are not significantly different. The inset shows C emission to export ratios across permafrost zones and mean emission to export ratios for Amazon[36], Yukon[12] and global river network[36,37] (assuming 0.9 Pg annual river C export to the oceans). We removed outliers to visually improve the graph, but run statistical analysis on the complete dataset. For sample size see Extended Data Table 2.
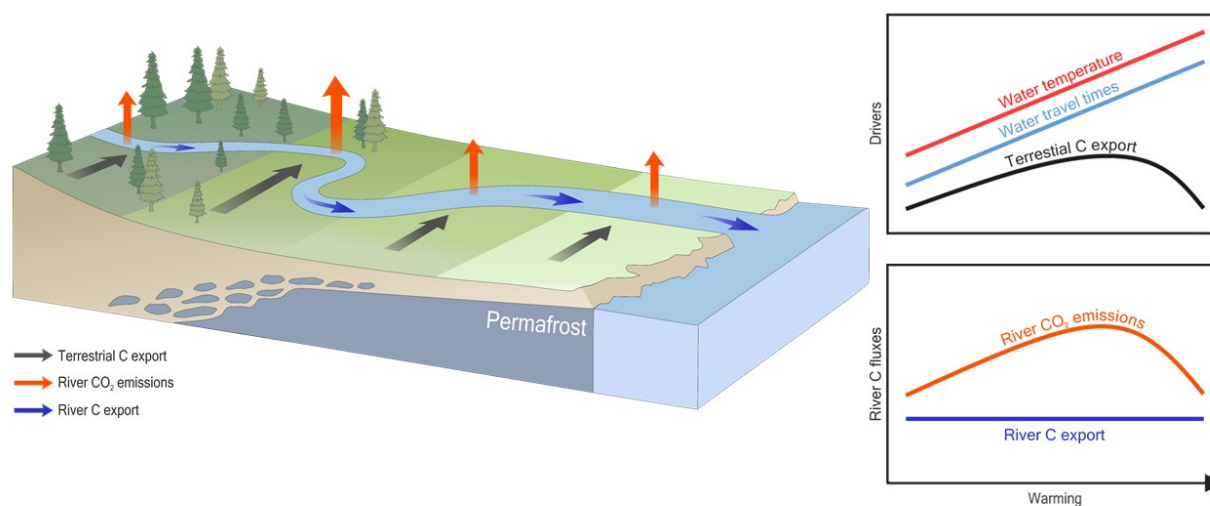
185

186
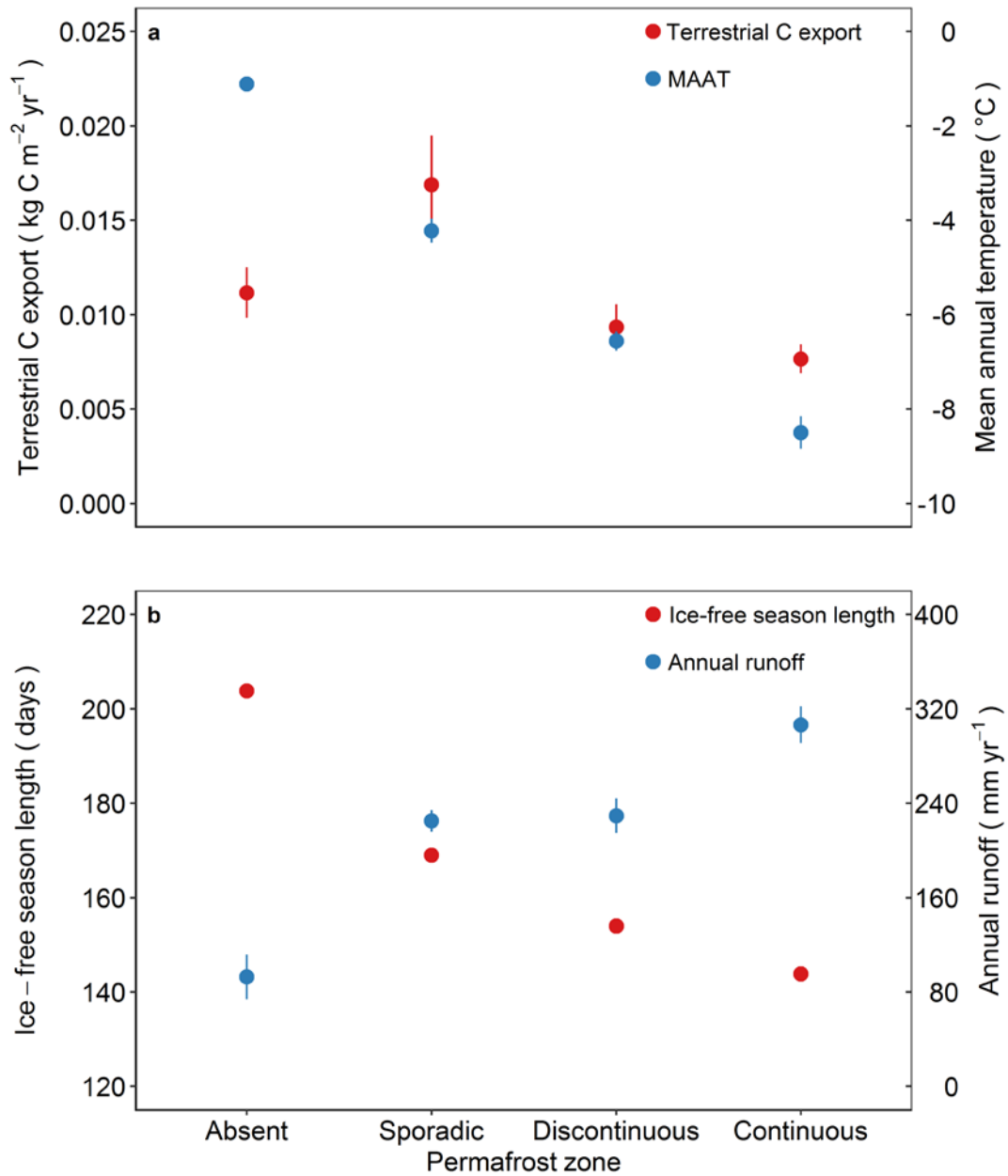
Fig. 3. (a) Terrestrial C export per unit catchment area and mean annual temperature, (b)

length of ice-free season and mean annual runoff across different permafrost zones. Dots

represent mean values while whiskers indicate standard error of the mean (SE). For sample size

see Extended Data Tables 1,2 and Supplementary Table 1.

191

192
Fig. 4. A conceptual model for changes in CO₂ emissions and downstream C export from permafrost-draining river network with warming. Warming raises water temperatures and extends river water travel times, resulting in increase in CO_2 emissions and emission to export ratios from river networks. Warming and associated permafrost thaw will likely also stimulate terrestrial C export, thus further enhancing riverine C fluxes. As warming progresses and permafrost disappears, terrestrial C export decreases, counteracting effects by temperature and water travel times, and leading to decrease in river CO_2 emissions.

200

201 **Methods:**

202 **Sampling sites.** The three studied river basins, Ob', Pur and Taz, are located in the Western

203 Siberian Lowland (WSL, Russia) between the southern taiga (56 °N) and the tundra (67 °N)

204 ecotones and represent an area of over 2,000,000 km^2. Because of its geographical location and

205 size, the region is distinct in terms of latitudinal and zonal variation of climate and permafrost

206 extent. The climate is moderate continental with mean annual air temperature (MAAT) ranging

207 from ca –0.5°C in the south to –9.5°C in the north and mean annual precipitation ranging from

208 477 (± 10, mean ± IQR) mm yr^{-1} to 444 (± 11, mean ± IQR) mm yr^{-1}, accordingly[31]. Permafrost

209 is widespread and occupies the greater part of the WSL, stretching from the polar circle to the

210 shores of the Arctic Ocean over 1,000 km distance[20,25]. The length of the ice cover period varies

211 latitudinally from 5 months in the south to more than 7 months in the north[38]. WSL is

212 characterized by a low and flat relief (0-200 masl)[39] and is dominated by Pliocene sands and

213 clays overlain by a layer of peat (ca 1-3 m)[31]. The thickness of seasonally frozen soil varies from

214 1.7-2 m in the south (55 °N) to less than 0.8 m in the north (66 °N)[40]. We sampled 58 streams

215 and rivers spanning a wide range of watershed sizes and permafrost extent. The catchment areas

216 of the sampled rivers ranged from 2 to 150,000 km^2, but exhibited relatively uniform

217 morphometry. The water flow was calm and lacked turbulence throughout the river course even

218 at peak discharge due to the overall flat terrain of WSL[31]. Our sampled sites showed no

219 systematic variation in watershed size, discharge or such landscape characteristics as proportion

220 of bogs or forests across different permafrost zones (for details on statistics see Statistical

221 analysis). We visited all sites during spring (10th-25th June) and summer (21th July-19th August)

222 2015. The timing of the two sampling campaigns covered ca 80% of annual water discharge

223   taking place in the basins[38], and therefore was assumed to be representative for the open water

224   season.

225   **Water chemistry.** At each location, pH, water temperature, dissolved oxygen saturation and

226   specific conductivity were measured below the water surface using a WTW® multiparameter

227   (uncertainty $\pm$ 5%). The probes were calibrated every other day using 2-point calibration

228   technique with standard buffer solutions. Air temperature and atmospheric pressure were

229   measured using ADC Summit handheld weather station (Silva®). Water samples for DOC, DIC,

230   nutrients, total nitrogen (TN) and total phosphorus (TP) (50 ml) were collected 1-2 m offshore

231   using vinyl gloves and pre-washed polypropylene (PP) jars. Samples for DOC and DIC were

232   filtered immediately on site using sterile plastic syringes in clean 30-mL PP Nalgene® bottles

233   through single-use pre-washed acetate cellulose filter units (Minisart®, Sartorius; 0.45 μm pore

234   size, 33 mm diameter). The first 20-50 mL of filtrate were discarded. DOC and DIC samples

235   were refrigerated in the dark until analysis by high-temperature catalytic oxidation using TOC-

236   VCSN, Shimadzu® (uncertainty $\pm$ 3%; 0.1 mg L^{-1} detection limit). The DOC blanks of filtrate

237   never exceeded 0.1 mg L^{-1}. Water samples for NH_4^+-N, NO_3^--N, and PO_4^{-3}-P were filtered on site

238   through pre-combusted (at 550° C for 4h) acid-washed glass fiber filters (0.45 µm, Whatman®

239   Arbor Technologies, USA) and were also stored frozen in the dark until analyses. These were

240   analyzed at Umeå University using an automated flow injection analyzer (FIA star 5000,

241   FOSS®, Denmark) with the detection limits 1 μg L^{-1} for NH_4^+-N, 0.5 μg L^{-1} for NO_3^--N and 0.5

242   μg L^{-1} for PO_4^{-3}-P, whereas TN and TP were analysed using IL 550 TOC/TN analyzer with the

243   detection limit of 50 μg L^{-1} (Hach-Lange GmbH®, Dusseldorf, Germany). Water samples for

244   dissolved CH_4 were collected in a 20-mL gastight vial closed without air bubbles using vinyl

245   stoppers and aluminium caps. 0.2 mL of saturated $HgCl_2$ was injected into the vial using two-

246 way needle system. Samples were stored in the dark until analysis in the laboratory at Tomsk

247 State University, where a headspace was made by displacing approximately 40% of water with

248 N_2 (99.999%) and creating two 0.5 mL replicate samples. These were analyzed using Bruker®

249 GC-456 gas chromatograph equipped with a flame ionization and thermal conductivity detectors.

250 Calibration of the detectors was performed after every 10th sample using air liquid gas standards

251 of known concentrations (0, 145 ppmv CH_4). The reproducibility of results was within ± 5%.

252 Molar concentrations of CH_4 were calculated by using temperature-specific solubility

253 coefficients as in Yamamoto et al.[41]. Because summer concentrations of dissolved CH_4 were

254 generally low (0.02 ± 0.02, mean ± IQR) and constituted ca 2% of total summer C emissions, the

255 data on CH_4 emissions are not discussed in this paper. We further measured ultraviolet

256 absorbance at 245 nm (UV_{245}) using a 1 cm quartz cuvette in a CARY-50 UV-VIS

257 spectrophotometer (Bruker®, UK). These values were later converted to UV_{254}[42]. We calculated

258 specific ultraviolet absorbance ($SUVA_{254}$) of the sampled water which served as a proxy for

259 aromatic C and organic matter quality in river water.

260 **pCO_2 concentrations.** Surface water partial pressure of CO_2 (pCO_2) was measured *in-situ* by

261 deploying a hand-held infrared gas analyzer (IRGA, GMT222 CARBOCAP probe, Vaisala®;

262 accuracy ± 1.5%) of various ranges (2 000, 10 000, 20 000 ppm) enclosed within a waterproof

263 and gas-permeable membrane. During the sampling, the hand-held meter was placed directly into

264 the water column of a sampled stream, where it was allowed to equilibrate for approximately 10

265 minutes. If the pCO_2 concentrations were 1.5% outside the sensor's range, it was replaced with

266 another sensor that had higher range. Sensor preparation was conducted in the lab following

267 method described by Johnson et al.[43]. The hand-held measurement indicator unit (MI70,

268 Vaisala®; accuracy ± 0.2%) was connected to the sensor allowing instantaneous readings of

269 $p\mathrm{CO}_2$. The replicates of readings were taken at each site to minimize uncertainty. The sensors

270 were calibrated linearly in the lab against standard gas mixtures (0, 800, 3 000, 8 000 ppm; $R^2 >$

271 0.99) after the sampling. The sensors' drift was 0.03-0.06% per day and the overall error was 4-

272 8% (relative standard deviation, RSD). Following calibration, the post-measurement correction

273 of the sensor output induced by changes in water temperature and barometric pressure was done

274 by applying empirically derived coefficients following Johnson et al.[43]. Finally, temperature-

275 specific solubility coefficients were used to calculate respective CO_2 concentrations in the water

276 as in Wanninkhof et al.[44].

277 **CO_2 flux calculations.** CO_2 flux (f_{CO_2}) was calculated using the following equation (Equation

278 1):

279 $$f_{CO_2} = K_h \, k_{CO_2} \left(C_{water} - C_{air} \right),$$ (1)

280 where K_h is the Henry's constant corrected for temperature and pressure (mol L^{-1} atm^{-1}), k_{CO_2} is

281 the gas exchange velocity at a given temperature (cm h^{-1}), C_{water} is the water CO_2 concentration,

282 and C_{air} is the CO_2 concentration in the ambient air.

283 To measure k_{CO_2}, we used a floating chamber. The chamber was made of a plastic bin (30 cm

284 length $\times$ 25 cm width $\times$ 15 cm height; volume 7.02 L) fitted with floats and covered with

285 aluminium tape to minimize surface heating. The chamber was connected to an IRGA and a

286 pump (GM70, Vaisala®) in a closed loop via CO_2-impermeable tubing and had a moisture trap

287 placed just before it. The pump was used to circulate air to the IRGA during the measurement

288 period. The hand-held measurement indicator unit (MI70, Vaisala®; accuracy $\pm$ 0.2%) was

289 attached to the system and used for recording values during the sampling. Prior to chamber

290 deployment it was flushed with ambient air for ca 20-30 sec. The chamber was gently placed on

291 the water surface near the shore to avoid inducing artificial turbulence. The $p\mathrm{CO}_2$ accumulation

292   rate inside the chamber was recorded continuously at 1-10 sec interval for 5-10 minutes.

293   Replicates of the measurements were done 2-3 times in different parts of the channel for each

294   location, when possible. If the river shore allowed free access, chamber measurements were

295   performed by allowing it to drift freely with the river current for some 50-200 m while recording.

296   In four of the rivers, where mean annual discharge is higher than 100 m^3 s^{-1} (Ob', Pyakupur, Pur

297   and Taz), the measurements were made by deploying the chamber alongside a boat during free

298   drift. 2-3 replicates of the measurements were made at each of the locations where the chamber

299   could drift. The rate of CO_2 accumulation was computed by linear regression. While 94% of the

300   measurements had a linear increase with $R^2 > 0.80$, 8% of the measurement had a linear increase

301   with $R^2 < 0.80$. These measurements were retained if the replicates existed and if the average R^2

302   between the replicates was greater than 50%. We further corrected for overestimation of the CO_2

303   accumulation rate inside the static chamber for each of the rates separately by multiplying with

304   the factor derived from average percent difference between drifting and static chamber

305   measurements. We manually trimmed readings from drifting chambers leaving only those, where

306   percent difference was negative (i.e. static chamber measurements were greater than the ones

307   obtained from the free drift). We did correction for each of the sampled sites and sampling

308   seasons separately. The correction reduced our measured CO_2 emissions on average by 33% in

309   spring and by 62% in summer, but did not affect the differences in annual CO_2 emissions among

310   permafrost zones. On four rivers (Ob', Pyakupur, Pur and Taz), we also measured pCO_2

311   concentrations and CO_2 emissions along with other water chemistry parameters (i.e. pH,

312   conductivity, dissolved O_2, etc.) from transects (4-5 points) across the river channel. None of the

313   measured parameters varied across the river channel for the corresponding rivers.

314   We estimated instantaneous CO_2 fluxes by modifying Equation 1 and using slopes of the CO_2

315   accumulation in the chambers (Equation 2):

316   $$f_{CO_2} = K_h \, h \left(\frac{d(pCO_2)}{dt} \right),$$ (2)

317   where h is chamber's mean height (m) while $d(pCO_2)/dt$ is the slope of CO_2 accumulation in

318   the chamber over time (ppm s^{-1})[23,45]. The k_{CO_2} values were then calculated by inverting Equation

319   1 and isolating k_{CO_2} (Equation 3)[45]:

320   $$k_{CO_2} = \frac{f_{CO_2}}{K_h \, (pCO_{2_{water}} - pCO_{2_{air}})},$$ (3)

321   where $pCO_{2_{water}}$ is the CO_2 concentration in the water (ppm), and $pCO_{2_{air}}$ is CO_2 air-water

322   equilibrium concentration set to 400 ppm, the average global atmospheric CO_2 concentration

323   during 2015. To compare gas transfer velocities among sites, calculated k_{CO_2} were then

324   standardized to a Schmidt number of 600 using the following equation (Equation 4)[23,45]:

325   $$k_{600} = k_{CO_2} \left(\frac{600}{Sc_{CO_2}} \right)^{-n},$$ (4)

326   where Sc_{CO_2} is CO_2 Schmidt number for a given temperature[45], exponent n is a coefficient that

327   describes water surface (2/3 for a smooth water surface regime while 1/2 for a rippled and a

328   turbulent one), and the Schmidt number for 20°C in freshwater is 600[23,46]. We used $n=2/3$

329   because all water surfaces of sampled rivers were considered flat and had a laminar flow.

330   Finally, we calculated k_{CH_4} and used these values to estimate instantaneous CH_4 emissions for

331   the respective rives.

332   **Stable water isotopes.** Samples for stable water isotopes (δ^2H and $\delta^{18}O$) were taken in the

333   middle of the river channel, or from the river bank at the depth of 0.5 m within the actively

334   flowing water. All samples were collected into 3.5 mL glass vials and stored in the dark at 4-6°C

335   until analysis. These were analysed at the University of Aberdeen using a Los Gatos® DLT-100

336   laser isotope analyzer with instrument precision of $\pm$ 0.4‰ for δ^2H and $\pm$ 0.1‰ for $\delta^{18}O$. Isotope

337   ratios are reported in the δ-notation using the Vienna Standard Mean Ocean Water standards.

338   **Ancillary data.** We used data on mean annual discharge, annual runoff, catchment area and

339   proportion of bogs, lakes, forest coverage and permafrost extent for each location from

340   Pokrovsky et al.[31]. We complemented this data with data on mean annual air temperature, mean

341   annual precipitation, mean length of ice cover season and topography of the watersheds using

342   data available in Russian literature[47,48].

343   **Annual river CO_2 emission.** We quantified annual river CO_2 emission as the product of mean

344   seasonal CO_2 emission and number of ice-free days for the respective rivers. Since the number of

345   sampled rivers in the absent area varied between the seasons (n=6 for spring and n=8 for

346   summer) and some of the rivers were sampled only during one of the seasons, we assumed

347   seasonal differences to be negligible for such rivers and used existing values when quantifying

348   annual river CO_2 emission (yielding a total n=9 for absent area). We, however, excluded such

349   rivers when analyzing seasonal differences in river CO_2 emission within each of the permafrost

350   zones (see Statistical analysis).

351   **Water surface area.** We modelled water surface area of the respective rivers by using published

352   relationships between the natural log of percent stream surface area and the natural log of mean

353   annual precipitation and MAAT for the watersheds above 60 °N[36] (Raymond et al., Equation 7

354   Supplementary Information):

355     $\ln(\%SA) = \ln P \ 1.04 - 5.01e^{-2} \ T - 7.08$,   (5)

356   where $\ln(\%SA)$ is the natural log of the percentage of stream surface area, $\ln P$ is the natural log

357   of mean annual precipitation in the watershed (mm yr^{-1}) while T is the MAAT (°C). These

358   calculated water surface areas were used to derive annual areal CO_2 emissions for each of the

359   studied sites. We acknowledge our estimate as rather conservative, but highlight it as being

360   realistic in reflecting summer base flow conditions for WSL rivers. It is likely that we

361   underestimate the areas because of large proportion of inundated floodplains during the spring

362   flood, when the flooded area ratio on average is 85% for WSL rivers excluding Taz[38]. These are

363   not accounted for in water surface areas calculations that largely rely on data of interannual

364   average of air temperature and precipitation in the respective catchments. However, we do not

365   attempt to derive high-resolution numbers; we rather seek to explore more general basin-scale

366   patterns that are not affected by year-to-year variability.

367   **River C export and Terrestrial C export.** We quantified river C export for each of the studied

368   sites as the product of summer DOC and DIC concentrations and site-specific discharge.

369   Comparing our values for organic C export with previously published estimates for 3 of our

370   WSL sites (Ob, Pur and Taz) measured at the rivers' outlets[10,31,47] gave similar results (1.7 ± 0.3,

371   mean of the difference $\pm$ interquartile range of the difference). Using a mass balance approach,

372   we calculated terrestrial C export for each catchment as the product of annual river CO_2

373   emissions and river C export.

374   **Statistical analysis.** Prior to statistical analyses, we grouped sampled rivers based on the

375   sampling location in four groups representing different permafrost zones: (i) absent (≤ 59 °N

376   n=9), (ii) sporadic (60-63 °N, n=27), (iii) discontinuous (64-65 °N, n=16) and (iv) continuous (>

377   65 °N, n=6). We merged isolated and sporadic permafrost zones together under sporadic

378   permafrost group as done elsewhere[6]. Further we classified sampled sites in four different classes

379   representing watershed sizes: (i) small (< 100 km^2, n=19), (ii) intermediate (100-1 000 km^2,

380   n=20), (iii) big (1 000-10 000 km^2, n=10) and (iv) huge (> 10 000 km^2, n=9). All statistical

381   analyses were performed in RStudio statistical software (Version 1.0.44, RStudio, Inc., <www. r-

382   project.org>).

383   To meet the normality assumption, all variables were transformed by using log transformation

384   when necessary. The normality of data distribution was assessed by Shapiro-Wilk normality test.

385   We further checked for homogeneity of variances between the groups by using parametric

386   Bartlett test. We used one-way analysis of variance (ANOVA) with Tukey's HSD post-hoc

387   comparisons to investigate differences in annual river CO_2 emissions among permafrost zones.

388   Both variables and their residuals followed normal distribution after transformation.

389   We further used linear mixed effects models (*lme4* package) when analyzing two-way

390   interactions of seasons and permafrost zones on the transformed per unit area daily CO_2

391   emissions and surface water pCO_2 concentrations. We used permafrost zones and seasons as

392   fixed factors that are expected to have a systematic influence on the data while we allowed our

393   sampled streams to randomly vary inside permafrost zone groups and watershed classes as well

394   as months inside permafrost zone groups to correct for nested design of the study and resolve

395   interdependency issue. In that way, we assumed that whatever the effects of permafrost extent

396   and seasons are, they are going to be the same for all rivers sampled within the permafrost zone

397   group. The best model fit was selected based on AIC. We also performed contrasts analyses on

398   respective mixed effects models by constructing orthogonal contrasts to compare seasons

399   between each other and avoid multiple comparisons (package *lsmeans*).

400   We used linear regression when analyzing the relationship between annual CO_2 emissions and

401   MAAT throughout permafrost zones. We also run multiple regression analysis on the dataset to

402   see which of the variables (i.e. discharge, annual runoff, proportion of bogs, lakes, forest

403 coverage and permafrost extent, etc.) can be good predictors of the seasonal and annual CO_2

404 emissions. No linear combination of the variables gave R^2 greater than 50%.

405 We further tested variation in watershed size, discharge or such landscape characteristics as

406 proportion of bogs and forest coverage among different permafrost zones groups by using

407 ANOVA with Tukey's HSD post-hoc comparison or a non-parametric alternative of Pairwise

408 Wilcox test with Holm adjustment. None of the variables exhibited significant differences

409 between permafrost zones. We also used parametric Levene's test on homogeneity of variances

410 when assessing variability in δ^2H and $\delta^{18}O$ between permafrost zones.

411 Note that we report untransformed data in the text, figures and tables. Because of non-normal

412 distribution of the data, we use mean ± interquartile range (IQR) when reporting uncertainty. All

413 statistical tests used a significance level of 5% ($\alpha = 0.05$) and were run on the complete dataset

414 including all rivers. We did remove outliers in Fig. 2 to visually improve the graph.

415 **Data Availability.** All data generated and analyzed during this study are included in this

416 published article (and its supplementary information files).

417 **References:**

418 1. Tarnocai, C. *et al.* Soil organic carbon pools in the northern circumpolar permafrost

419   region. *Global Biogeochem. Cycles* **23,** (2009).

420 2. Hugelius, G. *et al.* Estimated stocks of circumpolar permafrost carbon with quantified

421   uncertainty ranges and identified data gaps. *Biogeosciences* **11,** 6573–6593 (2014).

422 3. Schuur, E. A. G. *et al.* Climate change and the permafrost carbon feedback. *Nature* **520,**

423   171–179 (2015).

424 4. Crowther, T. W. *et al.* Quantifying global soil carbon losses in response to warming.

425   *Nature* **540,** 104–108 (2016).

426   5.   Smith, L. C. Siberian Peatlands a Net Carbon Sink and Global Methane Source Since the

427   Early Holocene. *Science (80-.).* **303,** 353–356 (2004).

428   6.   Vonk, J. E. *et al.* Reviews and syntheses: Effects of permafrost thaw on Arctic aquatic

429   ecosystems. *Biogeosciences* **12,** 7129–7167 (2015).

430   7.   Dorrepaal, E. *et al.* Carbon respiration from subsurface peat accelerated by climate

431   warming in the subarctic. *Nature* **460,** 616–619 (2009).

432   8.   Vonk, J. E. & Gustafsson, Ö. Permafrost-carbon complexities. *Nat. Geosci.* **6,** 675–676

433   (2013).

434   9.   Cole, J. J. *et al.* Plumbing the Global Carbon Cycle: Integrating Inland Waters into the

435   Terrestrial Carbon Budget. *Ecosystems* **10,** 172–185 (2007).

436   10.   Cooper, L. W. *et al.* Flow-weighted values of runoff tracers (δ18O, DOC, Ba, alkalinity)

437   from the six largest Arctic rivers. *Geophys. Res. Lett.* **35,** 3–7 (2008).

438   11.   Striegl, R. G., Aiken, G. R., Dornblaser, M. M., Raymond, P. A. & Wickland, K. P. A

439   decrease in discharge-normalized DOC export by the Yukon River during summer

440   through autumn. *Geophys. Res. Lett.* **32,** L21413 (2005).

441   12.   Striegl, R. G., Dornblaser, M. M., McDonald, C. P., Rover, J. R. & Stets, E. G. Carbon

442   dioxide and methane emissions from the Yukon River system. *Global Biogeochem. Cycles*

443   **26,** (2012).

444   13.   Denfeld, B. A., Frey, K. E., Sobczak, W. V., Mann, P. J. & Holmes, R. M. Summer CO_2

445   evasion from streams and rivers in the Kolyma River basin, north-east Siberia. *Polar Res.*

446   **32,** 1–15 (2013).

447   14.   Lundin, E. J., Giesler, R., Persson, A., Thompson, M. S. & Karlsson, J. Integrating carbon

448   emissions from lakes and streams in a subarctic catchment. *J. Geophys. Res.*

449   *Biogeosciences* **118,** 1200–1207 (2013).

450   15.   Abbott, B. W., Larouche, J. R., Jones, J. B., Bowden, W. B. & Balser, A. W. Elevated

451   dissolved organic carbon biodegradability from thawing and collapsing permafrost. *J.*

452   *Geophys. Res. G Biogeosciences* **119,** 2049–2063 (2014).

453   16.   Vonk, J. E. *et al.* High biolability of ancient permafrost carbon upon thaw. *Geophys. Res.*

454   *Lett.* **40,** 2689–2693 (2013).

455   17.   Dubois, K. D., Lee, D. & Veizer, J. Isotopic constraints on alkalinity, dissolved organic

456   carbon, and atmospheric carbon dioxide fluxes in the Mississippi River. *J. Geophys. Res.*

457   *Biogeosciences* **115,** (2010).

458   18.   Knoblauch, C., Beer, C., Sosnin, A., Wagner, D. & Pfeiffer, E. M. Predicting long-term

459   carbon mineralization and trace gas production from thawing permafrost of Northeast

460   Siberia. *Glob. Chang. Biol.* **19,** 1160–1172 (2013).

461   19.   Sheng, Y. *et al.* A high-resolution GIS-based inventory of the west Siberian peat carbon

462   pool. *Global Biogeochem. Cycles* **18,** (2004).

463   20.   Frey, K. E., Siegel, D. I. & Smith, L. C. Geochemistry of west Siberian streams and their

464   potential response to permafrost degradation. *Water Resour. Res.* **43,** (2007).

465   21.   Frappart, F. *et al.* Interannual variations of the terrestrial water storage in the Lower Ob'

466   Basin from a multisatellite approach. *Hydrol. Earth Syst. Sci.* **14,** 2443–2453 (2010).

467   22.   Romanovsky, V. E. *et al.* Thermal state of permafrost in Russia. *Permafr. Periglac.*

468   *Process.* **21,** 136–155 (2010).

469   23.   Alin, S. R. *et al.* Physical controls on carbon dioxide transfer velocity and flux in low-

470   gradient river systems and implications for regional carbon budgets. *J. Geophys. Res.* **116,**

471   G01009 (2011).

472   24.   Frey, K. E. Amplified carbon release from vast West Siberian peatlands by 2100.

473   *Geophys. Res. Lett.* **32,** L09401 (2005).

474   25.   Frey, K. E. & McClelland, J. W. Impacts of permafrost degradation on arctic river

475   biogeochemistry. *Hydrol. Process.* **23,** 169–182 (2009).

476   26.   Frey, K. E., McClelland, J. W., Holmes, R. M. & Smith, L. C. Impacts of climate warming

477   and permafrost thaw on the riverine transport of nitrogen and phosphorus to the Kara Sea.

478   *J. Geophys. Res. Biogeosciences* **112,** (2007).

479   27.   Hugelius, G. *et al.* The Northern Circumpolar Soil Carbon Database: spatially distributed

480   datasets of soil coverage and soil carbon storage in the northern permafrost regions. *Earth*

481   *Syst. Sci. Data* **5,** 3–13 (2013).

482   28.   Algesten, G. *et al.* Role of lakes for organic carbon cycling in the boreal zone. *Glob.*

483   *Chang. Biol.* **10,** 141–147 (2004).

484   29.   Ala-aho, P. *et al.* Using stable isotopes to assess surface water source dynamics and

485   hydrological connectivity in a high-latitude wetland and permafrost influenced landscape.

486   *J. Hydrol.* **556,** 279–293 (2017).

487   30.   Kawahigashi, M., Kaiser, K., Kalbitz, K., Rodionov, A. & Guggenberger, G. Dissolved

488   organic matter in small streams along a gradient from discontinuous to continuous

489   permafrost. *Glob. Chang. Biol.* **10,** 1576–1586 (2004).

490   31.   Pokrovsky, O. S. *et al.* Permafrost coverage, watershed area and season control of

491   dissolved carbon and major elements in western Siberian rivers. *Biogeosciences* **12,** 6301–

492   6320 (2015).

493   32.   Richey, J. E., Melack, J. M., Aufdenkampe, A. K., Ballester, V. M. & Hess, L. L.

494   Outgassing from Amazonian rivers and wetlands as a large tropical source of atmospheric

495   CO2. *Nature* **416,** 617–620 (2002).

496   33.   Zakharova, E., Kouraev, A. V., Rémy, F., Zemtsov, V. & Kirpotin, S. N. Seasonal

497   variability of the Western Siberia wetlands from satellite radar altimetry. *J. Hydrol.* **512,**

498   366–378 (2014).

499   34.   Smith, L. C. *et al.* Influence of permafrost on water storage in West Siberian peatlands

500   revealed from a new database of soil properties. *Permafr. Periglac. Process.* **23,** 69–79

501   (2012).

502   35.   Brown, J., O.J.J. Ferrians, J.A. Heginbottom & E.S. Melnikov. Circum-Arctic Map of

503   Permafrost and Ground Ice Conditions. (2001).

504   36.   Raymond, P. A. *et al.* Global carbon dioxide emissions from inland waters. *Nature* **503,**

505   355–359 (2013).

506   37.   Lauerwald, R., Laruelle, G. G., Hartmann, J., Ciais, P. & Regnier, P. A. G. Spatial

507   patterns in CO_2 evasion from the global river network. *Global Biogeochem. Cycles* **29,**

508   534–554 (2015).

509   38.   Zakharova, E. A. A. *et al.* The modern hydrological regime of the northern part of

510   Western Siberia from in situ and satellite observations. *Int. J. Environ. Stud.* **66,** 447–463

511   (2009).

512   39.   Karlsson, J. M., Lyon, S. W. & Destouni, G. Thermokarst lake, hydrological flow and

513   water balance indicators of permafrost change in Western Siberia. *J. Hydrol.* **464–465,**

514   459–466 (2012).

515   40.   Raudina, T. V. *et al.* Dissolved organic carbon and major and trace elements in peat

516   porewater of sporadic, discontinuous, and continuous permafrost zones of western Siberia.

517   *Biogeosciences* **14,** 3561–3584 (2017).

518   41.   Yamamoto, S., Alcauskas, J. B. & Crozier, T. E. Solubility of methane in distilled water

519   and seawater. *J. Chem. Eng. Data* **21,** 78–80 (1976).

520   42.   Cuthbert, I. D. & del Giorgio, P. Toward a standard method of measuring color in

521   freshwater. *Limnol. Oceanogr.* **37,** 1319–1326 (1992).

522   43.   Johnson, M. S. *et al.* Direct and continuous measurement of dissolved carbon dioxide in

523   freshwater aquatic systems-method and applications. *Ecohydrology* **3,** (2009).

524   44.   Wanninkhof, R. Relationship between wind speed and gas exchange over the ocean. *J.*

525   *Geophys. Res.* **97,** 7373–7382 (1992).

526   45.   Vachon, D., Prairie, Y. T. & Cole, J. J. The relationship between near-surface turbulence

527   and gas transfer velocity in freshwater systems and its implications for floating chamber

528   measurements of gas exchange. *Limnol. Oceanogr.* **55,** 1723–1732 (2010).

529   46.   Jähne, B., Heinz, G. & Dietrich, W. Measurement of the diffusion coefficients of

530   sparingly soluble gases in water. *J. Geophys. Res. Ocean.* **92,** 10767–10776 (1987).

531   47.   Gordeev, V. V., Martin, J. M., Sidorov, I. S. & Sidorova, M. V. A reassessment of the

532   Eurasian river input of water, sediment, major elements, and nutrients to the Arctic Ocean.

533   *Am. J. Sci.* **296,** 664–691 (1996).

534   48.   Nikitin, S. P. & Zemtsov, V. A. The Variability of Hydrological Parameters of Western

535   Siberia. Nauka, Novosibirsk, 204 pp., (1986) (available in Russian literature).

536   49.   Novikov, S. M. et al. Hydrology of Bog Territories of the Permafrost Zone of Western

537   Siberia. BBM publishing House, St. Petersburg, 535 pp., (2009) (available in Russian

538   literature).

539

540

549

550   **Author contribution:** J.K. and O.S.P. contributed to study design. S.N.K. organized sampling

551   campaigns and logistics. S.S., R.M.M., I.V.K. and V.K. contributed to sampling. L.S.S. analyzed

552   DOC and DIC samples. S.G.K. complemented data with literature material. S.S. analyzed data,

553   prepared figures and tables. S.S., J.K., O.S.P. and H.L. wrote the paper. C.S., D.T. and P.A.

554   helped with results interpretation. All authors commented on the manuscript and have no

555   conflicts of interest to declare.

556

557   **Competing financial interests:** The authors declare no competing financial interests.

558 **Materials & Correspondence:** Supplementary Information is available in the online version of

559 the paper. Reprints and permissions information is available at www.nature.com/reprints.

560 Correspondence and requests for materials should be addressed to S.S.

561 (svetaserikova22@gmail.com) or J.K. (jan.p.karlsson@umu.se).

562

563   **Extended data**
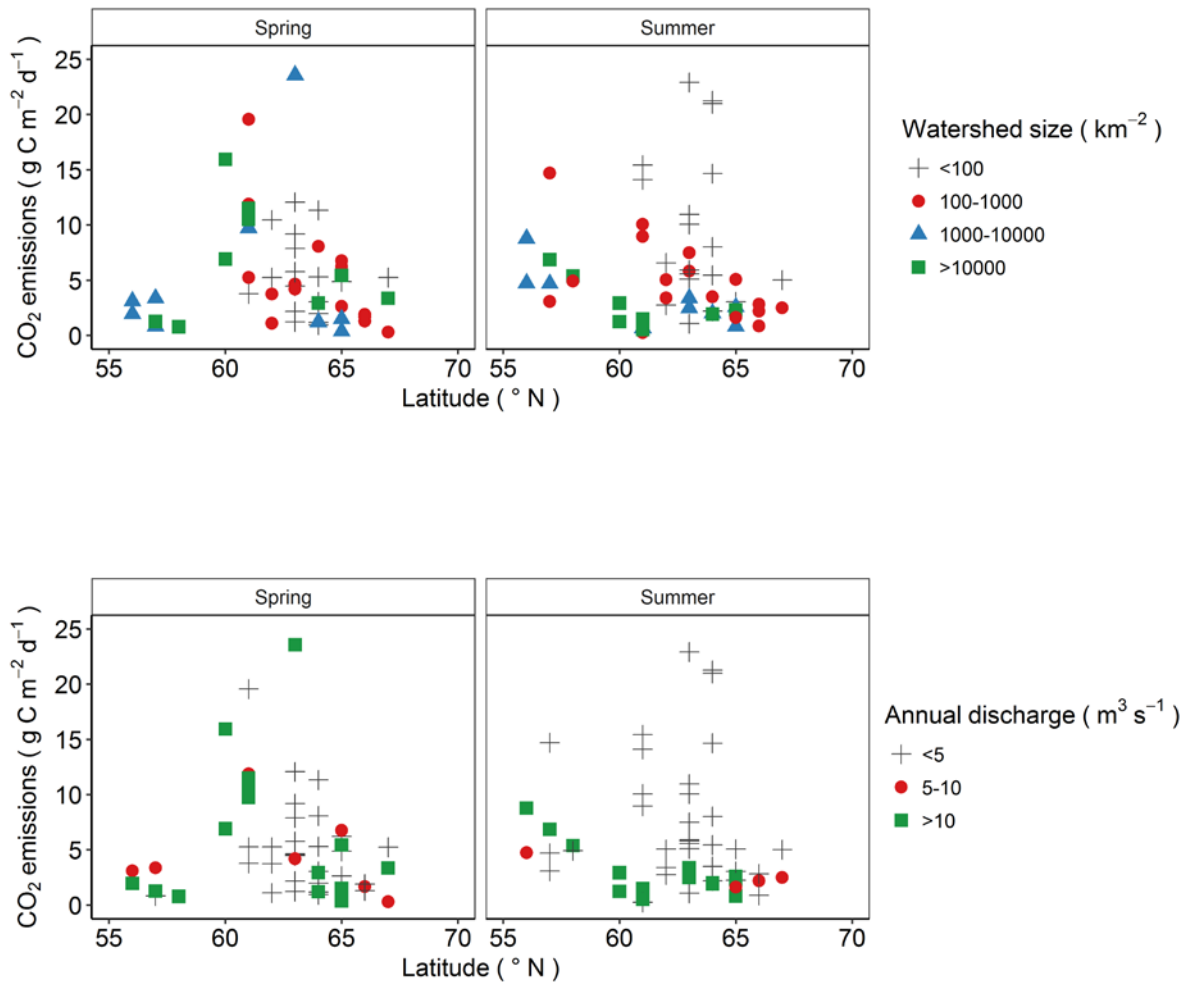
565   **Fig. 1. Seasonal CO₂ emissions per unit water area grouped based on watershed classes and**

566   **annual discharge plotted against latitude.** Watershed classes and annual discharge groups are

567   shape- and color coded.

568
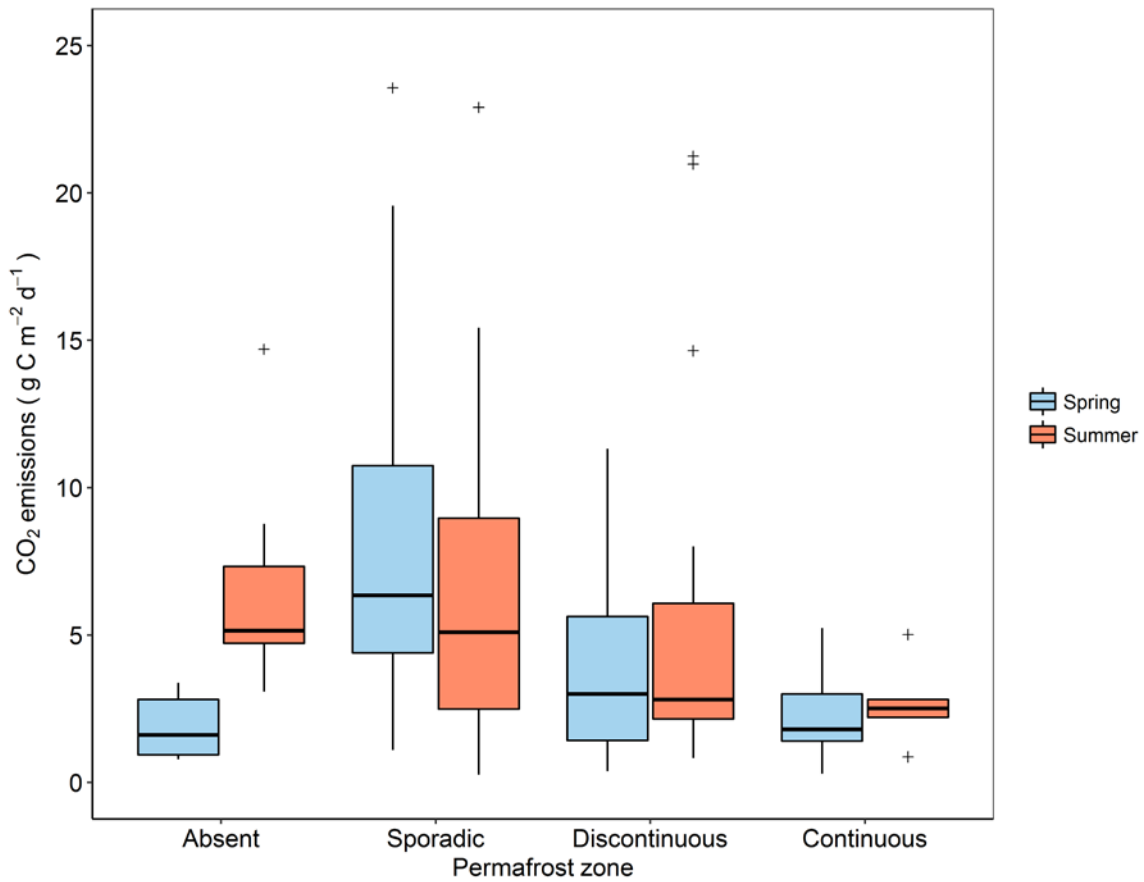
569
Fig. 2. Seasonal CO₂ emissions per unit water area across different permafrost zones. Boxes
are bound by 25th and 75th percentiles. Whiskers show 1.5 interquartile range (IQR). Solid line
represents median values while crosses indicate outliers. For sample size see Extended Data
Table 1.

575
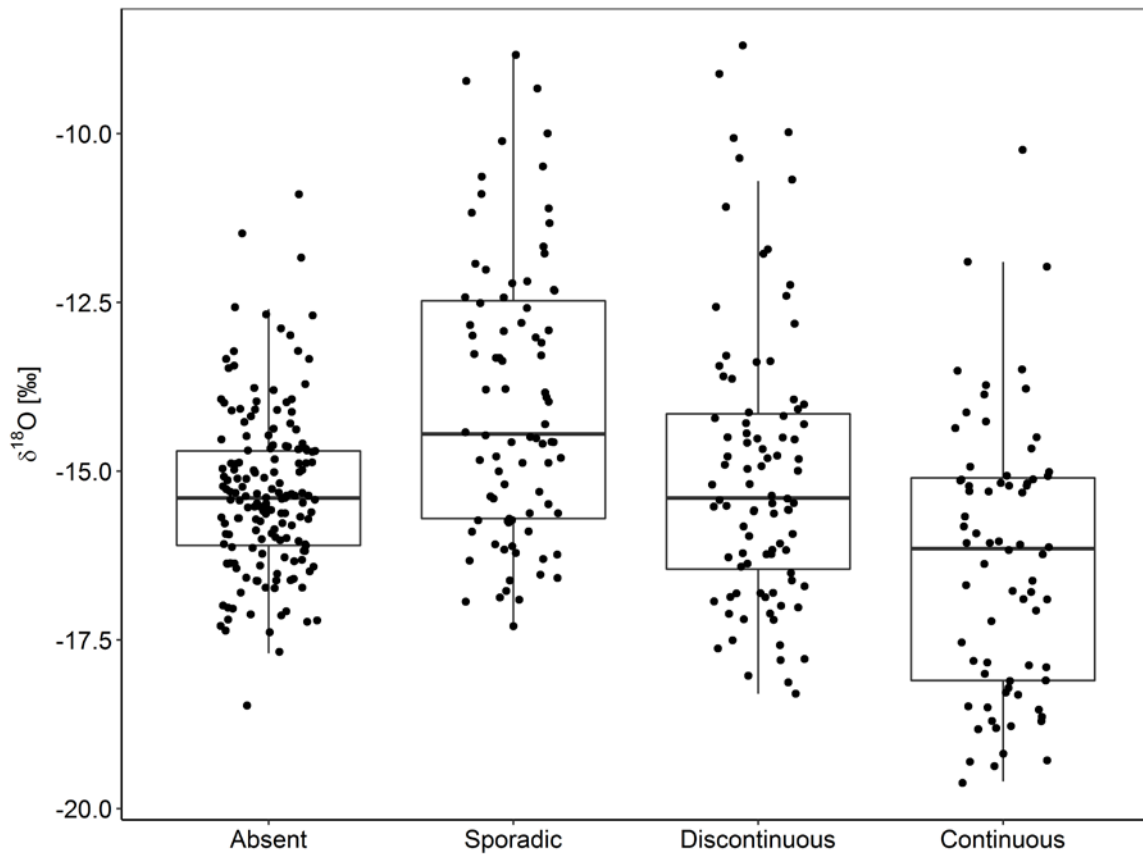
Fig. 3. River δ¹⁸O across different permafrost zones. Boxes are bound by 25ᵗʰ and 75ᵗʰ

percentiles. Whiskers show 1.5 interquartile range (IQR) while solid line represents median

values. The isotope variability is lower in permafrost-free zone ($F = 13.6$, $P < 0.05$) suggesting

deeper flow-paths in permafrost-free soils. In other permafrost zones, the isotope variability is

greater, implying a more rapid hydrological response, when water flow is restricted to overland

flow and has shorter travel times.

582

583 **Table 1. Mean seasonal surface water chemistry parameters and emission rates per unit of**

584 **water area (± interquartile range, IQR) across permafrost zones.** Dash stands for missing

585 values.

	Permafrost zone							
	Absent		Sporadic		Discontinuous		Continuous	
	Spring	Summer	Spring	Summer	Spring	Summer	Spring	Summer
n	6	8	26	26	16	16	6	5
pCO$_2$, µatm	3511 (± 287)	5328 (± 2397)	5072 (± 1615)	4997 (± 1745)	4155 (± 2998)	4274 (± 4345)	2402 (± 502)	2187 (± 53)
CO$_2$ flux, g C m^{-2} d^{-1}	1.8 (± 1.8)	6.6 (± 2.6)	12.0 (± 7.2)	7.5 (± 7.2)	3.9 (± 4.2)	6.0 (± 3.9)	2.2 (± 1.6)	2.6 (± 0.6)
n	9	7	26	27	16	16	6	6
DOC, mg L^{-1}	29.0 (± 24.2)	21.3 (± 16.2)	16.9 (± 7.4)	16.7 (± 9.3)	12.2 (± 2.8)	14.6 (± 4.8)	11.8 (± 1.4)	14.3 (± 3.6)
DIC, mg L^{-1}	14.1 (± 5.6)	56.1 (± 31.8)	2.1 (± 1.5)	4.1 (± 2.7)	1.6 (± 1.4)	2.7 (± 1.4)	2.4 (± 1.3)	7.5 (± 2.0)
DOC:DIC ratio	2.4 (± 2.7)	0.5 (± 0.5)	15.9 (± 12.4)	9.1 (± 10.4)	12.9 (± 6.2)	9.6 (± 4.3)	5.4 (± 3.2)	2.1 (± 0.2)
n	9	4	26	22	16	16	6	6
Conductivity, µS cm^{-1}	150.4 (± 33.0)	523.2 (± 72.7)	50.7 (± 23.2)	66.1 (± 24.0)	35.9 (± 18.7)	41.1 (± 22.2)	45.6 (± 31.2)	94.1 (± 23.2)
pH	7.4 (± 0.2)	7.6 (± 0.1)	5.8 (± 0.6)	6.1 (± 0.7)	6.0 (± 0.8)	5.9 (± 0.8)	6.5 (± 0.4)	7.1 (± 0.2)
n	6	-	25	3	12	-	-	-
CH$_4$, mg L^{-1}	0.008 (± 0.00)	-	0.02 (± 0.02)	0.02 (± 0.03)	0.04 (± 0.03)	-	-	-
n	6	-	23	3	11	-	-	-
CH$_4$ flux, g C m^{-2} d^{-1}	0.03 (± 0.02)	-	0.27 (± 0.19)	0.01 (± 0.01)	0.25 (± 0.17)	-	-	-
n	3	4	26	24	16	16	6	6
SUVA$_{254}$	3.2 (± 0.9)	3.2 (± 0.2)	4.5 (± 0.4)	4.6 (± 0.4)	4.3 (± 0.5)	4.5 (± 1.1)	3.9 (± 0.3)	3.9 (± 0.4)

586

587

588   **Table 2. Mean annual river C fluxes per unit water area and mean annual terrestrial flux**

589   **per unit catchment area (± interquartile range, IQR) across permafrost zones.**

	Permafrost zone			
	Absent	Sporadic	Discontinuous	Continuous
n	9	26	16	6
*River CO_2 emissions, kg C m^{-2} yr^{-1}	1.02 (± 0.36)	1.65 (± 1.14)	0.78 (± 0.52)	0.36 (± 0.21)
River C export, kg m^{-2} yr^{-1}	1.03 (± 0.47)	0.72 (± 0.26)	0.46 (± 0.18)	0.69 (± 0.21)
River C emission:export	1.18 (± 0.36)	2.65 (± 2.29)	1.80 (± 1.80)	0.56 (± 0.31)
Terrestrial C export, kg m^{-2} yr^{-1}	0.011 (± 0.004)	0.016 (± 0.011)	0.009 (± 0.003)	0.007 (± 0.002)

590
591   *For River CO_2 emissions in the sporadic permafrost zone n=27.
592

593

594   **Table 3. Summary of water chemistry parameters (mean of summer ± interquartile range,**

595   **IQR of summer) across permafrost zones.**

	Permafrost zone			
	Absent	Sporadic	Discontinuous	Continuous
n	9	26	16	6
O_2, mg L^{-1}	6.75 (± 4.40)	7.44 (± 2.37)	8.75 (± 3.40)	12.16 (± 0.70)
n	9	27	16	6
DIN, mg L^{-1}	0.20 (± 0.25)	0.06 (± 0.05)	0.07 (± 0.05)	0.05 (± 0.05)
TN, mg L^{-1}	1.28 (± 0.35)	0.82 (± 0.45)	0.68 (± 0.10)	0.71 (± 0.28)
TOC, mg L^{-1}	37.55 (± 41.00)	23.96 (± 8.50)	18.93 (± 6.87)	18.58 (± 5.75)
PO_4, mg L^{-1}	0.03 (± 0.04)	0.02 (± 0.01)	0.02 (± 0.01)	0.04 (± 0.02)
TP, mg L^{-1}	0.19 (± 0.05)	0.15 (± 0.10)	0.19 (± 0.10)	0.16 (± 0.07)
n	8	26	16	6
TC, mg L^{-1}	1.25 (± 0.59)	1.95 (± 1.44)	1.77 (± 1.01)	3.84 (± 4.13)

596

597

598

Supplementary Materials:

600

Supplementary Table 1. Data generated and analyzed during this study. DD represents

decimal degrees. NA stands for missing values.

603

Supplementary Table 2. Statistical results of orthogonal contrasts. Between-seasons

comparison of pCO$_2$ concentrations. For details on statistics see Supplementary Info Statistical

analysis.

Contrast	Estimate	SE	df	t.ratio	p.value
Spring_Absent-Summer_Absent	0.156	0.103	109.000	1.507	0.134
Spring_Sporadic-Summer_Sporadic	-0.021	0.053	109.000	-0.400	0.689
Spring_Discontinuous-Summer_Discontinuous	-0.029	0.067	109.000	-0.436	0.663
Spring_Continuous-Summer_Continuous	-0.0411	0.116	109.000	-0.354	0.723

607

Supplementary Table 3. Statistical results of orthogonal contrasts. Between-seasons

comparison of CO$_2$ emissions. The star indicates statistically significant difference at 0.05 level.

For details on statistics see Supplementary Info Statistical analysis.

Contrast	Estimate	SE	df	t.ratio	p.value
Spring_Absent-Summer_Absent	0.579	0.215	66.465	2.690	0.009*
Spring_Sporadic-Summer_Sporadic	-0.246	0.108	52.145	-2.276	0.026*
Spring_Discontinuous-Summer_Discontinuous	0.131	0.137	50.221	0.951	0.345
Spring_Continuous-Summer_Continuous	0.153	0.237	54.790	0.643	0.522

611